



**HAL**  
open science

## Permeability enhancement of HDR reservoirs by hydraulic fracturing

Murad S. Abuaisha, B. Loret

► **To cite this version:**

Murad S. Abuaisha, B. Loret. Permeability enhancement of HDR reservoirs by hydraulic fracturing. 14th International Conference of the International Association for Computer Methods and Advances in Geomechanics, Sep 2014, Kyoto, Japan. pp.1681-1686. hal-02460875

**HAL Id: hal-02460875**

**<https://minesparis-psl.hal.science/hal-02460875>**

Submitted on 30 Jan 2020

**HAL** is a multi-disciplinary open access archive for the deposit and dissemination of scientific research documents, whether they are published or not. The documents may come from teaching and research institutions in France or abroad, or from public or private research centers.

L'archive ouverte pluridisciplinaire **HAL**, est destinée au dépôt et à la diffusion de documents scientifiques de niveau recherche, publiés ou non, émanant des établissements d'enseignement et de recherche français ou étrangers, des laboratoires publics ou privés.

# Permeability enhancement of HDR reservoirs by hydraulic fracturing

M. AbuAisha & B. Loret

*Laboratoire 3SR, Institut National Polytechnique de Grenoble, Grenoble, France*

**ABSTRACT:** The permeability of geothermal reservoirs needs to be enhanced. Hydraulic Fracturing (HF) is the standard tool used for that purpose. Here HF is introduced in a thermo-poroelastic framework. The main ingredient of the HF scheme is a fracturing model that governs the evolution of the size and width of the fractures. At any geometrical point, a fracture-induced anisotropic permeability tensor is calculated: next to the injection pressure, the directional properties of this tensor are strongly influenced by the geological stresses. This fracturing model is integrated into a domestic Fortran 90 finite element code. Circulation tests and thermal recovery from the enhanced geothermal reservoir of Soultz–Sous–Forêts are simulated.

## 1 INTRODUCTION

The exploitation of the geothermal energy has become a world strategy since 1975. However, geothermal energy exploitation has been limited to certain areas on the planet where it was feasible and easy to extract, for instance areas near tectonic plate boundaries. Modern technologies such as hydraulic fracturing and chemical enhancement were recently deployed to extract geothermal energy from specific geological sites, if cost effective (Turcotte & Schubert 2002).

Geothermal energy is produced by pumping cold fluids into Hot Dry Rock (HDR) reservoirs where temperature gradients are favorable. Deep in the ground at the level of the reservoir, the thermo-poroelastic mechanisms that are taking place will be controlling the development of reservoir fluid pressure, the effective stresses, the rate of fluid losses, the thermal recovery progress and hence the economic viability of the entire geothermal process (Bruehl 1995). One of the most important factors affecting thermal recovery from HDR reservoirs is the permeability of the fractured medium. Natural HDR reservoirs have quite low permeability; the process of injecting geothermal fluids is always endangered by large amounts of fluid loss and frustratingly inefficient thermal recovery. Modern geothermal projects are nowadays focusing on enhancing the permeability of the geothermal reservoirs which has given rise to the terminology of Enhanced Geothermal Systems (EGS). This enhancement is implemented by pumping geothermal fluids at considerable flow rates which will eventually lead reservoir fractures to evolve and connect (Hydraulic Fracturing (HF)). Representation of thermal recovery from a single fracture embed-

ded in a geothermal reservoir has been outlined by (Cheng, Ghassemi, & Detournay 2001). The same approach has been addressed by (Zhou, Ghassemi, & Cheng 2009) with investigating the thermoelastic and poroelastic effects of cold water injection.

Studies that are addressing the evolution of HDR reservoir permeability under thermo-poroelastic conditions are scarce. For instance, (Lee & Ghassemi 2010) considered HDR reservoirs consisting of a single fracture and adopted empirical relations to relate permeability to the effective stresses. Such studies, despite being indicative, do not address the effect of HF on the stability of geothermal boreholes, nor do they study the dependence of HF process on the geostatic conditions of the HDR reservoirs.

This paper provides a fracturing model which is integrated into a fully coupled thermo-poroelastic framework. This fracturing model is capable of tracking the fracture evolution at any geometrical point and in all possible fracture orientations. The new fracture properties namely, fracture radius and aperture, are used to calculate local fluid velocity fields using Navier–Stokes equation for laminar flow. The macroscopic velocity field is deduced by a directional averaging over the local velocities. An anisotropic permeability tensor, that describes the hydraulic connectivity of the hydraulically fractured medium, is then calculated by applying Darcy's law for laminar flow.

## 2 HYDRAULIC FRACTURING (HF)

In a poroelastic medium, HF can be defined as the process of causing fractures to propagate by using pressurized fluid. Normally the process of HF is suppressed by the confining pressure coming from

the surroundings. HF is practically done by reducing the effective stress by pumping pressurized fluid to a point the minimum principal stress (in algebraic sense) becomes tensile and exceeds the tensile strength of the rock. HF is henceforth synonymous to tensile failure of rock material.

## 2.1 Thermal effects on HF

Thermally induced fracturing is a phenomenon observed while injecting cold water into hot rock layer. Rock matrix shrinks and thus reduces the compressive geologic stresses that confine the borehole. Let us consider the stress equation which describes the thermo–mechanical behavior of a saturated porous medium subjected to a temperature change  $\Delta T$ :

$$\sigma_{ij} + \kappa p \delta_{ij} = E_{ijkl} (\varepsilon_{kl} - \varepsilon_{kl}^T), \quad (1)$$

$\sigma_{ij}$  is the total stress tensor,  $p$  is the pore fluid pressure,  $\kappa$  is the Biot's coefficient,  $\delta_{ij}$  is the Kronecker delta,  $E_{ijkl}$  is the elasticity tensor,  $\varepsilon_{kl}$  is the mechanical strain tensor,  $\varepsilon_{kl}^T$  is the thermal strain tensor defined as  $\varepsilon_{kl}^T = (\alpha_s/3) \Delta T \delta_{kl}$  and  $\alpha_s$  is the cubical thermal expansion coefficient.

If the porous medium was sufficiently permeable to a point the diffusion of fluid happens much faster than the diffusion of heat (the common case when simulating real EGS reservoirs), the term  $\kappa p \delta_{ij}$  could be assumed constant while cooling. Thus, while cooling  $\Delta T$  becomes negative and contractive mechanical strains ( $\varepsilon_{kl}$ ) are needed in equation (1) to keep the equilibrium condition  $\nabla_j \sigma_{ij} = 0$ . Contractive mechanical strains develop positive tensile stresses, imagine some degree of restraint at the boundaries, which in turn means reduction of the confining compressive geologic stresses.

## 2.2 Hydraulic Fracturing Model (HFM)

This section is aimed at providing a fracturing model which is capable of ensuring a directionally stable mode I of fracture evolution.

### 2.2.1 Fracture initiation

To illustrate the concept of fracture initiation, let us consider the following situation: a vertical borehole penetrating a rock formation which is homogeneous and isotropic in its elastic and transport properties. The far field stresses are such that  $-\sigma_v > -\sigma_H > -\sigma_h$ . As the injection starts, the rock formation cools and the wellbore pressure  $p_w$  increases. The effective tangential stress  $\sigma'_\theta$  in the rock material will correspondingly decrease, see figure (1).

The condition for HF initiation reads:

$$\sigma'_\theta = T_c, \quad (2)$$

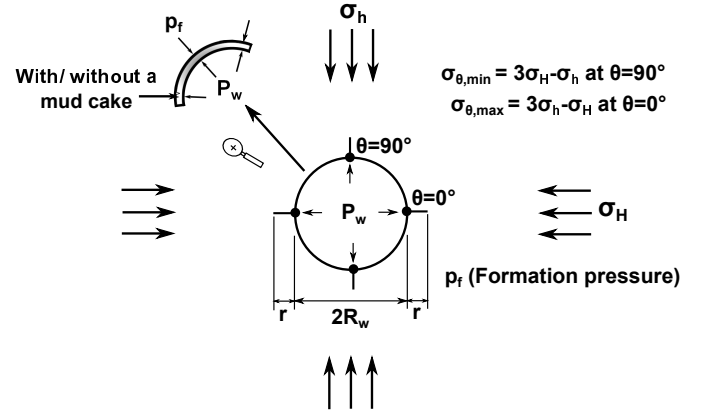


Figure 1: Vertical wellbore with vertical cracks. Wellbore wall can/can not be lined with a mud cake.

where  $T_c$  is the material tensile strength. In the presence of a mud cake, the wellbore pressure required to create the hydraulic fracturing in the direction of  $\sigma_H$  is expressed as in equation (3):

$$p_w^{\text{HF}} = - \left[ (3\sigma_h - \sigma_H) + p_f - \frac{E \alpha_s \Delta T}{3(1 - \nu)} - T_c \right]. \quad (3)$$

In the absence of a mud cake and if the pressurization rate was slow enough to ensure steady state conditions during pumping, the pressure required to create hydraulic fracturing is given by<sup>1</sup>:

$$p_w^{\text{HF}} = - \left[ (1 - \nu)(3\sigma_h - \sigma_H) + (1 - 2\nu)p_f - \frac{E \alpha_s \Delta T}{3} - (1 - \nu)T_c \right]. \quad (4)$$

Note that the pressurization of impermeable media (permeability  $< 10^{-18} \text{ m}^2$ ) is equivalent to the presence of a mud cake. Meanwhile all porous media with permeability  $> 10^{-18} \text{ m}^2$  are assumed permeable and the limit for pressurization without a mud cake shall apply.

Summing up the foregoing strategies, HF technique in EGS can be summarized following figure (2). As the injection of cold water begins, the geostatic stresses start to decrease. Temperature change (cooling) helps mitigating the compressive geostatic stresses as well. If pressurization and cooling continue to a point the effective stresses become tensile and exceed the tensile strength of the rock material, fracturing takes place.

### 2.2.2 Fracturing criterion

Let us consider again the vertical borehole of figure (1) with a group of cracks of average radius  $r$  and arbitrary normal direction  $\mathbf{n}$  in the horizontal plane  $(x, y)$ . If the borehole pressure is gradually increased

<sup>1</sup>To understand the role of thermal stresses in equations (3) and (4), the reader is advised to check (AbuAisha 2014) and (Fjaer et al. 2008).

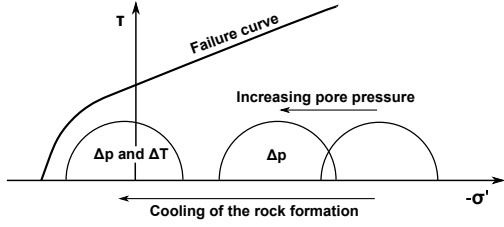


Figure 2: Mohr circles and failure line: the effect of increasing pore pressure and decreasing temperature on HF.

to a point the effective stress  $\sigma'_n$  (at the crack tip) becomes tensile and exceeds the limit of material tensile strength, the group of cracks starts propagating and consequently the average aperture of cracks increases.

The following model, equation (5), has been suggested to track the evolution of average radius  $r$  of a group of cracks in direction  $\mathbf{n}$ :

$$F(\sigma'_n, r) = f(r) \sigma'_n \sqrt{\pi r} - K_{Ic}, \quad (5)$$

where  $K_{Ic}$  is the material toughness for mode I of fracturing. The normal effective stress applied to the crack ( $\sigma'_n$ ) is expressed as:

$$\sigma'_n = n_i \sigma'_{ij} n_j. \quad (6)$$

$f(r)$  is a positive scalar valued function which controls the kinetics of crack propagation.  $f(r)$  is expressed as:

$$f(r) = \begin{cases} \eta \left( \frac{r_f}{r} \right), & r < r_f \\ \eta, & r \geq r_f \end{cases} \quad (7)$$

with  $r_f$  denoting the critical crack radius for accelerated coalescence of microcracks, and  $\eta$  being the crack growth stabilizing parameter.  $f(r)$  decreases as the crack begins to propagate denouncing the relaxation of local tensile stresses as the cracks grow away from the zone of stress concentration: this feature ensures the stable growth of cracks. As the cracks start to coalesce, the function  $f(r)$  reaches an asymptotic value: this feature marks the onset of damage localization and macroscopic failure.

The loading-unloading condition for a propagating crack of normal direction  $\mathbf{n}$  is defined according to the Kuhn-Tucker relations:

$$\dot{r} \geq 0, \quad F(\sigma'_n, r) \leq 0, \quad \dot{r} F(\sigma'_n, r) = 0. \quad (8)$$

Authors like (Klimczak et al. 2010) and (Shao, Zhou, & Chau 2005) have related the normal increment of crack aperture to crack face mismatch and local grain matrix interaction during crack growth. Thus, the normal crack aperture increment is proportional to the average crack radius increment, that is to say:

$$\frac{\delta w}{\delta r} = \beta, \quad (9)$$

where  $\beta$  is the proportionality coefficient. (Klimczak et al. 2010) have performed experiments and collected data from literature on 15 types of rocks. They have found that  $\beta$  ranges from 0.0005 to 0.5.

### 2.2.3 Permeability tensor

Knowing the new fracture radius  $r(\mathbf{n})$  and aperture  $w(\mathbf{n})$  of arbitrary direction  $\mathbf{n}$ , the local velocity field is calculated by implementing Navier-Stokes equation for laminar flow between two parallel plates. The macroscopic velocity field is deduced by a directional averaging over the local velocities. An anisotropic permeability tensor, that describes the fracture hydraulic connectivity, is then calculated by applying Darcy's law for laminar flow:

$$\mathbf{k}_c = \frac{N}{\Omega} \frac{1}{48} \int_S R(\mathbf{n}) w(\mathbf{n})^3 r(\mathbf{n})^2 (\boldsymbol{\delta} - \mathbf{n} \otimes \mathbf{n}) dS, \quad (10)$$

where  $N/\Omega$  is the fracture density. The connectivity coefficient  $R(\mathbf{n})$  is given by:

$$R(r(\mathbf{n})) = t_1 \left( \frac{r(\mathbf{n}) - r_0}{r_f - r_0} \right)^{t_2}, \quad 0 \leq R(\mathbf{n}) \leq t_1, \quad (11)$$

where  $r_0$  is the initial crack radius.  $R(r(\mathbf{n}))$  involves two dimensionless positive constants,  $t_1$  and  $t_2$ , to be determined. The value of this coefficient depends on the microstructure of the damaged material. It indicates that connectivity between cracks increases as the cracks grow in size, which contributes to the crack permeability tensor  $\mathbf{k}_c$ .

The overall permeability tensor of the cracked medium is composed of two parts: the initial permeability tensor denoted as  $\mathbf{k}_0$  due to the initial porosity, and the crack induced permeability tensor denoted by  $\mathbf{k}_c$ . The flow in the two cavities is assumed to take place in parallel and the total permeability tensor is obtained by summation, i.e.  $\mathbf{k} = \mathbf{k}_0 + \mathbf{k}_c$ .

## 3 HYDRAULIC STIMULATION

The HDR reservoir of Soultz–Sous–Forêts is chosen to be hydraulically enhanced by our HFM model discussed above. To perform the stimulation process, the HFM is integrated into a domestic Fortran 90 finite element code that simulates thermo–poroelastic transient BVPs.

### 3.1 Geometry and material properties

Due to symmetry, only a quarter of the reservoir volume is to be simulated, figure (3). Initial and boundary conditions are also highlighted on the graph. The horizontal finite element mesh is composed of 300 Q4 elements, 10 elements in  $y$ -direction and 30 elements in  $x$ -direction. The simulations are conducted under a 2D plane strain conditions.

Cold water is injected from the well (GPK1) and left to travel through the geothermal reservoir before it is retrieved via the production well (GPK2). Injection pressure is increasing at GPK1 linearly; pumping starts with 58 MPa and terminates, after 15 years, with 82 MPa.

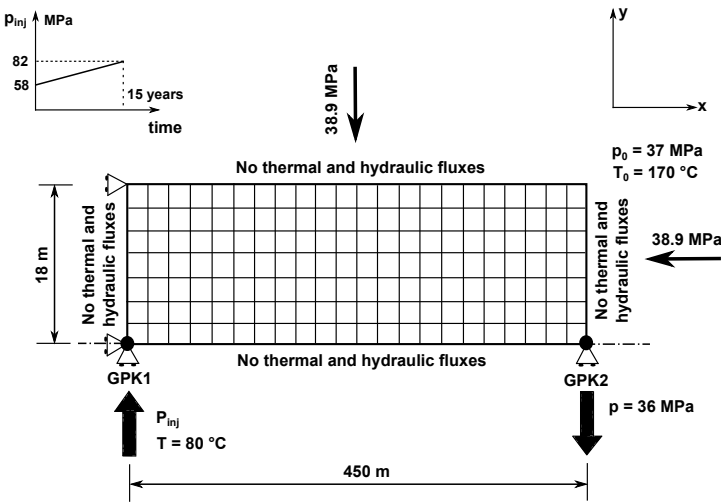


Figure 3: Modeling of HF process at Soultz-Sous-Forêts. Figure is not to scale.

The material properties of Soultz-Sous-Forêts reservoir are shown in Tables (1) and (2). The crack growth stabilizing parameter  $\eta$  is determined based on the threshold of HF by equation (4). Circulation tests for a time period of 1 year with and without standing for HF are reported below.

### 3.2 Results and simulations

The high fluid gradients near the injection well traveling mainly in  $y$ -direction (the shorter dimension of the reservoir) cause fast cooling and lead cracks to propagate and thus permeability to increase in this direction, figures (4) and (5).

Since the reservoir is constrained in  $x$  and  $y$  directions due to roller displacement, near the injection well  $y = x = 0$  m, cooling creates tensile stresses which mitigate geologic stresses and contribute to crack propagation in these directions, figures (9) and (10).

In the case when HF is utilized, the distribution of effective stress is much more irregular following the preferential cooling derived by the new paths created by the HF, see figures (9) and (10) and compare with figure (4).

In the regions where HF is active, formation pressure distribution tends to be spatially uniform before

it starts to decline considerably in the regions of low permeability, figures (7) and (8). This pattern of pressure distribution was also noticed by (Lee & Ghassemi 2010).

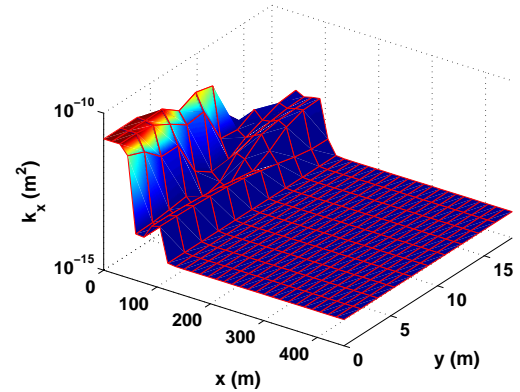


Figure 4: Space distribution of longitudinal permeability component  $k_x$  at year 1 of HF.

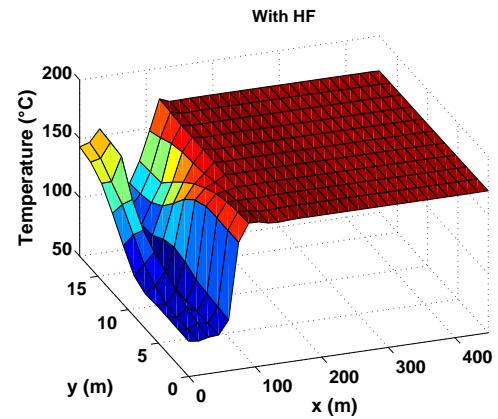


Figure 5: Temperature space distribution at year 1 with HF.

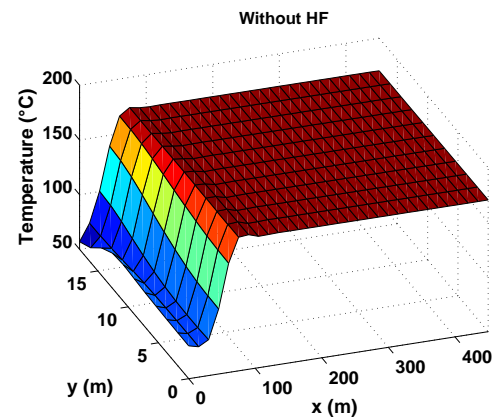


Figure 6: Temperature space distribution at year 1 without HF.

Figure (11) shows the space distribution of the longitudinal permeability component  $k_x$  at year 10 of HF. The reservoir is being enhanced equally in  $x$  and  $y$  directions. This is due to the isotropic geologic stress state applied on the reservoir, see figure (3).

Table 1: Material properties of Soultz–Sous–Forêts reservoir, (Evans et al. 2009).

Property	Value
Drained Young's modulus $E$	$54 \times 10^9$ (Pa)
Drained Poisson's ratio $\nu$	0.25
Bulk modulus of solid grains $K_s$	$50 \times 10^9$ (Pa)
Bulk modulus of fluid $K_f$	$2.2 \times 10^9$ (Pa)
Dynamic viscosity of the fluid $\mu$	$3 \times 10^{-4}$ (Pa.s)
Porosity $\phi$	0.1003
Initial permeability $k_0$	$6.8 \times 10^{-15}$ (m <sup>2</sup> )
Solid thermal conductivity $\chi_s$	2.49 (W/m°C)
Fluid thermal conductivity $\chi_f$	0.6 (W/m°C)
Solid heat capacity at constant volume $c_{s,v}$	1000 (J/kg °C)
Fluid heat capacity at constant volume $c_{f,v}$	4200 (J/kg °C)
Density of solid $\rho_s$	2910.2 (kg/m <sup>3</sup> )
Unit weight of water $\gamma_f$	9800 (N/m <sup>3</sup> )
Volumetric thermal expansion of the solid $\alpha_s$	$7.5 \times 10^{-6}$ (1/°C)
Volumetric thermal expansion of the fluid $\alpha_f$	$1 \times 10^{-3}$ (1/°C)

Table 2: Parameters used in the application of the HFM. References: 1.(Shao, Zhou, & Chau 2005), 2.(Atkinson 1991) and 3.(Evans et al. 2009).

	Parameter	Value	Reference
Damage parameters	Initial radius of cracks $r_0$ (cm)	15.0	3
	Final radius of cracks $r_f$ (cm)	55.0	3
	Initial aperture of cracks $w_0$ (cm)	$3.111 \times 10^{-3}$	Calculated
	Material tensile strength $T_c$ (MPa)	8.3	2
	Material toughness $K_{Ic}$ (MPa√m)	1.87	2
	Crack growth stabilizing parameter $\eta$	0.04	Parameterized
	Crack density (1/m <sup>3</sup> )	$2 \times 10^6$	1
Hydraulic connectivity parameters	$t_1$	0.0001	1
	$t_2$	1.0	1

If the applied geologic stress state is not isotropic, which is the common case in field, fractures will evolve in the direction of maximum geologic stress. The permeability will, therefore, be enhanced in that direction (AbuAisha 2014).

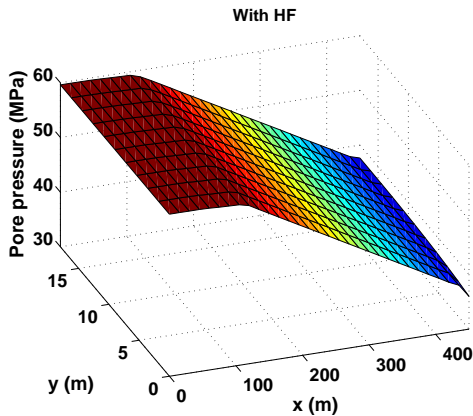


Figure 7: Pressure space distribution at year 1 with HF.

Still, the anisotropy of the permeability remains limited. The ratio of anisotropy between the principal values along the  $x$  and  $y$  directions remains in the range [0.4, 2.5] as observed by (Schulze, Popp, & Kern 2001).

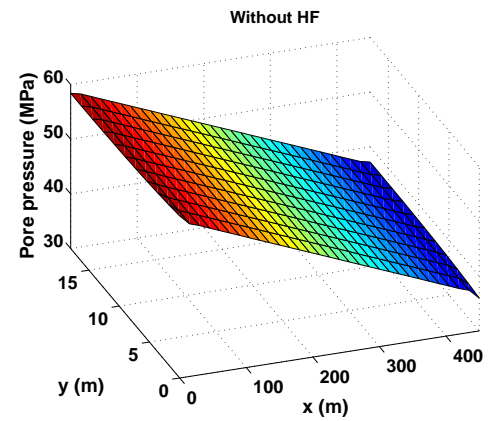


Figure 8: Pressure space distribution at year 1 without HF.

## 4 CONCLUSION

Hydraulic fracturing in a thermo–poroelastic framework has been studied in the context of thermal recovery from large scale geothermal systems. A fracturing model which is capable of tracking the directional evolution of fractures has been presented. This fracturing model has been integrated into a domestic Fortran 90 FEM code which is able to solve thermo–poroelastic transient BVPs.

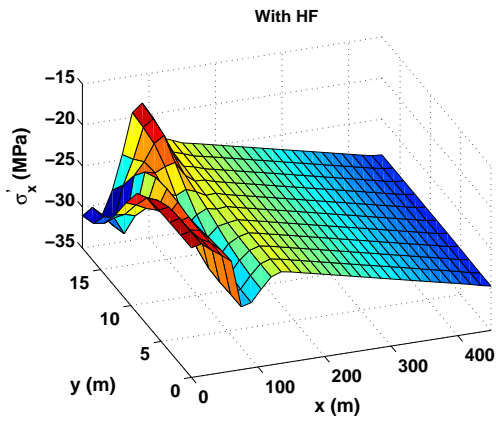


Figure 9: Space distribution of longitudinal effective stress  $\sigma'_x$  at year 1 with HF.

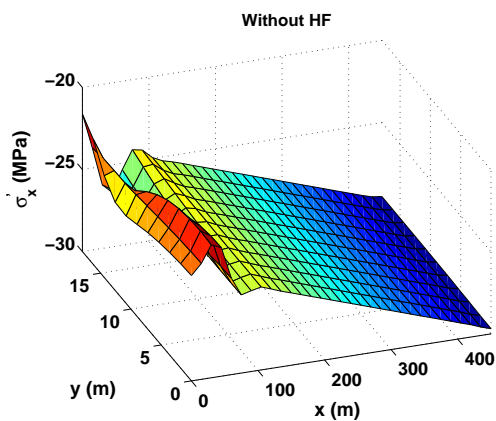


Figure 10: Space distribution of longitudinal effective stress  $\sigma'_x$  at year 1 without HF.

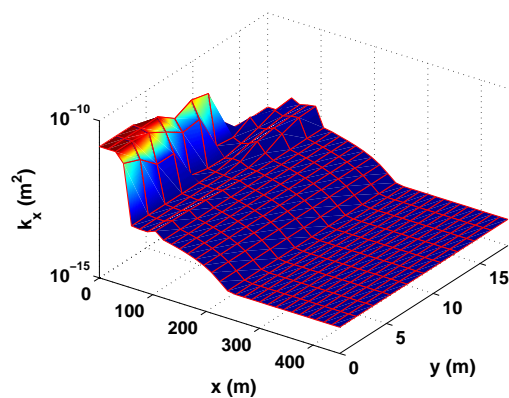


Figure 11: Space distribution of longitudinal permeability component  $k_x$  at year 10 of HF.

## REFERENCES

- AbuAisha, M. (2014, April). Enhanced Geothermal Systems (EGS): Permeability stimulation through hydraulic fracturing in a thermo-poroelastic framework. PhD thesis, Université de Grenoble, France.
- Atkinson, B. K. (1991). *Fracture mechanics of rock* (second printing ed.). London, Great Britain: Academic Press Limited.
- Bruel, D. (1995). Heat extraction modelling from forced fluid flow through stimulated fractured rock masses: Application to the Rosemanowes hot dry reservoir. *Geothermics* 24(3),

361–374.

- Cheng, A. H.-D., A. Ghassemi, & E. Detournay (2001). Integral equation solution of heat extraction from a fracture in hot dry rock. *International Journal for Numerical and Analytical Methods in Geomechanics* 25, 1327–1338.
- Evans, K., B. Valley, M. Häring, R. Hopkirk, C. Baujard, T. Kohl, T. Mégel, L. André, S. Portier, & F. Vuataz (2009). Studies and support for the EGS reservoirs at Soultz–Sous–Forêts. Technical report, Centre for Geothermal Research – CREGE, CHYN, University of Neuchâtel.
- Fjaer, E., R. M. Holt, P. Horsrud, A. M. Raaen, & R. Risnes (2008). *Petroleum related rock mechanics* (second ed.). Radarweg 29, 1000 AE Amsterdam, The Netherlands: Elsevier B.V.
- Klimczak, C., R. A. Schultz, R. Parashar, & D. M. Reeves (2010). Cubic law with aperture-length correlation: Implications for network scale fluid flow. *Hydrogeology Journal* 18(4), 851–862.
- Lee, S. H. & A. Ghassemi (2010, 1–3 February). Thermo-poroelastic analysis of injection-induced rock deformation and damage evolution. In *Proceedings of the Thirty-Fifth Workshop on Geothermal Reservoir Engineering*, Stanford University, Stanford, California.
- Schulze, O., T. Popp, & H. Kern (2001). Development of damage and permeability in deforming rock salt. *Engineering Geology* 61, 163–180.
- Shao, F. J., H. Zhou, & K. T. Chau (2005). Coupling between anisotropic damage and permeability variation in brittle rocks. *International Journal for Numerical and Analytical Methods in Geomechanics* 29, 1231–1247.
- Turcotte, D. L. & G. Schubert (2002). *Geodynamics*. (second ed.). Cambridge, England, UK: Cambridge University Press.
- Zhou, X. X., A. Ghassemi, & A. H.-D. Cheng (2009). A three-dimensional integral equation model for calculating poro- and thermoelastic stresses induced by cold water injection into a geothermal reservoir. *International Journal for Numerical and Analytical Methods in Geomechanics* 33, 1613–1640.